Available online at www.sciencedirect.com
SCIENCE DIRECT®
Journal of Solid State Chemistry 177 (2004) 866–874
JOURNAL OF SOLID STATE CHEMISTRY
http://elsevier.com/locate/jssc

The synthesis mechanism of $Ca_3Al_2O_6$ from soft mechanochemically activated precursors studied by time-resolved neutron diffraction up to 1000°C

J.M. Rivas Mercury,[a,1] A.H. De Aza,[a] X. Turrillas,[b,2] and P. Pena[a,*]

[a] *Instituto de Cerámica y Vidrio, CSIC, Campus de Cantoblanco, Camino de Valdelatas s/n, Madrid 28049, Spain*
[b] *E. Torroja Institute for Construction Sciences (IETcc), CSIC, Cl. Serrano Galvache s/n., Madrid 28033, Spain*

Received 29 June 2003; received in revised form 15 September 2003; accepted 23 September 2003

Abstract

The reaction pathway for the $Ca_3Al_2O_6$ formation up to 1300°C, from mechanochemically treated mixtures of amorphous aluminum hydroxide and $CaCO_3$, was studied *in situ* by differential thermal analysis, constant heating rate dilatometry and time-resolved neutron powder diffraction. The experiment was carried out, in an open system, on a sample with the nominal $Ca_3Al_2O_6$ stoichiometry. The results obtained by neutron diffractometry and thermal analysis were in good agreement with the data obtained by scanning electron microscopy and X-ray diffraction on heat-treated and-quenched samples. The synthesis path implied the formation of cryptocrystalline Al_2O_3, crystalline CaO, $CaAl_2O_4$ and $Ca_{12}Al_{14}O_{33}$ as transitory phases. Finally the nucleation and growth of the single phase $Ca_3Al_2O_6$ took place at 1300°C and exhibited porous structure due to CO_2 and H_2O release.

Keywords: Neutron thermodiffractometry; Solid-state reactions; $Ca_3Al_2O_6$; Mechanochemical synthesis; Processing

1. Introduction

The ternary oxide $Ca_3Al_2O_6$ is cubic, S.G. Pa3, with $a = 1.5263$ nm [1]. It is one of the minor (5–10%) components of Portland cement. This compound readily reacts with water in a few seconds to yield, through a tortuous path, which involves the formation of short-life hydrates [2], the stable cubic hydrate $Ca_3Al_2(OH)_{12}$. This reaction like all hydration processes associated with the different calcium aluminates is exothermic. However, $Ca_3Al_2O_6$ is quite difficult to synthesize as a pure phase, being often accompanied by small amounts of CaO or $Ca_{12}Al_{14}O_{33}$ (also known as mayenite). Among the numerous reports published on the synthesis of $Ca_3Al_2O_6$, there is some confusion, or at least inconsistencies, mainly about the intermediate phases. For example, Williamson and Glasser [3] reported $Ca_{12}Al_{14}O_{33}$ to be the principal non-equilibrium phase, although $CaAl_2O_4$ was also observed. In a later publication, Singh et al. [4] also mentioned the presence of several aluminate phases such as $CaAl_4O_7$, $CaAl_2O_4$ and $Ca_{12}Al_{14}O_{33}$. Finally, it is worth alluding to a recent work by Mohamed and Sharp [5] dealing with the synthesis mechanism of $Ca_3Al_2O_6$ in the range from 1150 to 1350°C using quantitative X-ray diffraction analysis. They observed the formation of $Ca_{12}Al_{14}O_{33}$ and $CaAl_2O_4$ as transient phases. According to their experimental data, the kinetics mechanism of $Ca_3Al_2O_6$ formation from oxides follows a diffusion-controlled model of Ginstling–Brounshtein type [6], the activation energy for the reaction being 220 ± 10 kJ/mol. These authors proposed that the rate-determining step is the diffusion of Ca^{2+} ions through the layers of reaction products, whereas the Al^{3+} ions remain relatively immobile.

Bearing in mind the discordances described and that the process seemed to be controlled by diffusion, it was considered of interest to attempt the synthesis route

*Corresponding author. Instituto de Cerámica y Vidrio, CSIC, Campus de Cantoblanco, Arganda del Rey 28500, Madrid, Spain.
E-mail address: ppena@icv.csic.es (P. Pena).
[1] Permanent address: Centro Federal de Educação Tecnológica do Maranhão, CEFET-MA, Av. Getúlio Vargas, 04, Monte Castelo, CEP 65025-001, São Luís, MA, Brazil.
[2] Also at European Synchrotron Radiation Facility (ESRF), BP 220, Grenoble Cedex F-38043, France.

0022-4596/$ - see front matter © 2003 Elsevier Inc. All rights reserved.
doi:10.1016/j.jssc.2003.09.022

from very finely divided precursors. That is why an unconventional "soft" mechanochemical synthesis route is undertaken. This method implies a mechanochemical treatment of the starting powders (reaction mixtures) in a liquid media containing hydroxyl groups, i.e. water or various alcohols. Indeed, the use of carbonates and/or hydroxides mixtures (at least one of this would contain water or hydroxyl groups and/or carbonate groups), is an attractive alternative to synthesize calcium aluminates [7–9]. This hard wearing treatment (e.g. high-energy ball milling or shearing) provokes a massive proliferation of crystal defects (such as dislocations, grain boundaries, etc.) into formerly perfect or nearly perfect single crystal domains.

This paper deals with the reaction mechanism of $Ca_3Al_2O_6$ formation in soft mechanochemically treated mixtures of amorphous aluminum hydroxide ($Al(OH)_3$) with calcite ($CaCO_3$), placing special emphasis on the 600–950°C temperature region. Indeed, this interval of temperatures is not very well known, is critical for the final synthesis of tricalcium aluminate and to the best of our knowledge this is the first time an *in situ* probing technique (neutron thermodiffractometry) has been used to explore it.

2. Experimental

2.1. Ceramic processing

The starting materials used in this investigation were: analytical grade amorphous aluminum hydroxide (Alfa Aesar, Jonhson Matthey, Germany) and crystalline $CaCO_3$, calcite (Merck, Germany). Table 1 shows the chemical analysis and physical properties of these raw materials.

The appropriate amounts of $CaCO_3$ and amorphous $Al(OH)_3$ according to the stoichiometry of Eq. (1) were milled and homogenized by attrition with MgO-partially stabilized zirconia balls in isopropyl alcohol media.

$$3CaCO_3 + 2Al(OH)_3 \rightarrow Ca_3Al_2O_6 + 3H_2O(g) + 3CO_2(g). \quad (1)$$

After milling, the powders were dried, sieved (60 μm) and conformed into $\simeq$10 mm diameter bars isostatically cold pressed at 50 MPa. Differential thermal analysis and thermogravimetric analysis studies (DTA-TG, STA 409, Netzsch, Germany) were conducted, on green compacted samples, at a constant heating rate of 2°C/min up to 1300°C, in air, using Pt crucibles. Their sintering behavior, between room temperature and 1300°C was determined in a dilatometer (Setsys 16/18, Setaram, France) with α-alumina support on 20 mm long specimens at a heating rate of 2°C/min. Additional isothermal treatments were performed in an electric furnace (Super-Kanthal, 1700°C, Switzerland), at temperatures from 800 to 1300°C programming 2°C/min ramps for both heating and cooling. The phase composition of compacts was determined by X-ray diffraction—Cu$K\alpha$ radiation—(XRD, Siemens D-5000, Kristalloflex, Germany).

Table 1
Chemical analysis of starting materials expressed in wt%

Chemical species/property	$CaCO_3$	$Al(OH)_3$
SiO_2	na	0.25
TiO_2	na	0.01
Al_2O_3	0.009	53.2
CaO	55.8	0.12
MgO	0.08	0.02
Na_2O	$\leqslant$0.2	$\leqslant$0.2
K_2O	0.012	0.01
Fe_2O_3	0.0007	0.01
SO_4^{2-}	0.01	na
Ignition loss	43.75	46.00
Mineralogical analysis	Calcite	Amorphous
Specific surface BET (mg)	0.20	39.0
Particle size d_{50} (μm)	13.80	6.25
Empirical density (Pic. He)(g/cm^3)	2.69	2.20

Species not determined are indicated by na.

Microstructural analysis and phase identification was done by scanning electron microscopy (Zeiss DSM 950, Germany) with an energy dispersive X-ray analyzer (SEM-EDS) on samples coated with gold by sputtering, polished and thermally etched. To back up the reaction mechanism proposed, free energy computations for all the possible reactions between CaO and Al_2O_3 were performed using HSC [10]. This is a computing package that offers an exhaustive thermochemical database and includes enthalpy (H), entropy (S) and heat capacity (C) data for chemical compounds.

2.2. Neutron thermodiffraction

The high-temperature powder neutron diffraction experiments were carried out at the Institute Laue–Langevin, (ILL) Grenoble, France, in Instrument D1B ($\lambda = 0.25227$ nm). A furnace was employed to reach temperatures up to 1000°C. The heating element, a vanadium cylinder, induced a constant temperature area of several centimeters along its axis. The temperature was continuously recorded and controlled with two chromel–alumel thermocouples of an accuracy of 5°C, located next to the heating element. Approximately 5 g of polycrystalline specimen lightly compacted were introduced into a quartz cylindrical tube of 10 mm diameter and 800 mm high which was kept open to the atmosphere during the whole experiment. This way a uniform heat distribution in the whole sample was assured. Diffraction patterns were accumulated every 300 s during the heating ramp whose temperature was raised at a rate of $\simeq$1.5°C/min. These acquisition

conditions mean a 10°C temperature resolution for each pattern. For a more specific technical description see Ref. [11].

2.3. Data processing

The data treatment details were described in a previous paper [11]. General plotting was carried out with the help of the commercial package Origin [12]. The visualization of data in the form of 3D plots and contour maps was made with the help of a commercial package, NOeSYS [13]. To measure intensities, reflections were fitted to Gaussian curves with in-house procedures written in IDL [14].

3. Results

3.1. Effects of grinding

The particle size distributions of the $CaCO_3$—amorphous $Al(OH)_3$ mixture at the 3:2 molar ratio after one and 30 min of milling were monomodal (see Fig. 1). As shown in the figure, d_{50}, particle/agglomerate size values changed with milling time from 6.27 to 1.98 μm. The maximum size of the 90 wt% of the particles, d_{90}, was also strongly dependent on the milling process and decreased from 15.6 to 4.17 μm. This latter parameter is critical for the reactivity of the compacted powders. The initial specific surface area, was 10.5 m^2/g, after the attrition milling processing, rose to 19.4 m^2/g. Given the optimal characteristics of powders milled for 30 min, they were chosen to study its reaction mechanism. The real density after milling was 2.47 g/cm^3. On the other hand X-ray diffraction did not indicate any increase of amorphous phases; no variations of peak intensities was observed as a consequence of the mechanochemical treatment (30 min of grinding).

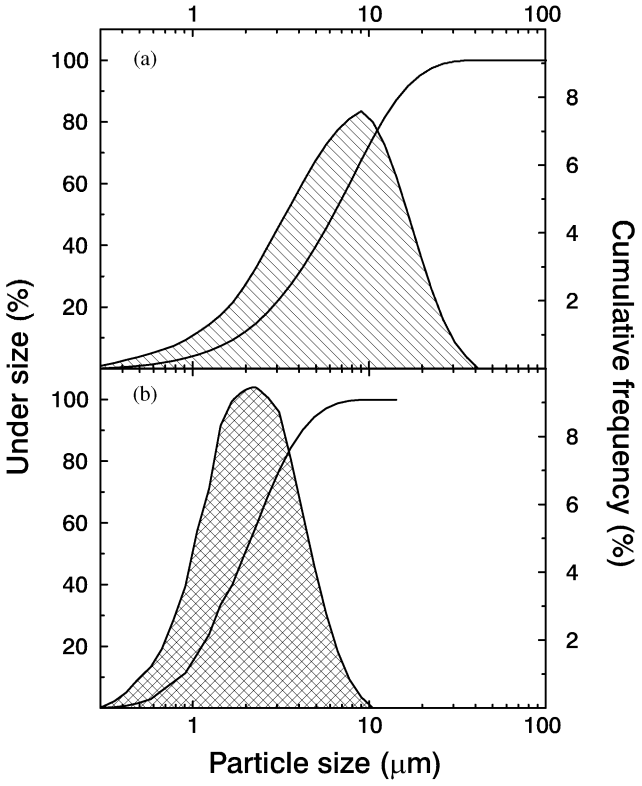

Fig. 1. Effect of milling on the average particle size, d_{50}, of the $CaCO_3$—amorphous $Al(OH)_3$ mixture. The size distribution, before and after 30 min of treatment is represented by (a) and (b), respectively.

3.2. Thermal analysis

In Fig. 2(a), it can be appreciated that the sample lost a total weight of 45% in two clear stages of 16% and 29%, respectively. Those stages matched two endothermic peaks. The first one, very broad, with a minimum at ≃123°C can be assigned to amorphous $Al(OH)_3$ dehydration and the second with the minimum at 784°C to a CO_2 release [18,4]. Furthermore, two clear exothermic peaks at 437°C and ≃916°C and finally another very small and broad effect at about 1181°C can be seen. The exothermal effect at ≃437°C is due to the combustion of the small amounts of isopropyl alcohol from the milling process physically adsorbed to the particles surface. The thermal effects at 916°C and 1181°C can be attributed to $Ca_{12}Al_{14}O_{33}$ and $CaAl_2O_4$ formation, respectively.

The constant heating rate dilatometric curve has been represented in Fig. 2(b). This sample suffered three shrinkage effects: the first one between 125 and 325°C, the second with the maximum between 800°C and 915°C and the last one at 1165°C.

3.3. X-ray and neutron diffraction

To understand the reaction mechanism during the high-temperature synthesis of $Ca_3Al_2O_6$ from a $CaCO_3$—$Al(OH)_3$ mixture in a 3:2 molar ratio, the above mentioned *in situ* neutron diffraction patterns were used. The real-time evolution of the mixture as a function of temperature can be seen in the 3D diagram of Fig. 3(a). To visualize events, such as diffraction shifts or collapse of phases, more precisely, a contour map in two dimensions was projected from the 3D graph. See Fig. 3(b). The existence of phase domains is clearly highlighted by their diffraction peaks shown in the figure with the corresponding Miller indices. The contour maps of Fig. 3(b) clearly show that the break-up of calcite structure takes place at temperatures higher than 700°C. As expected, the calcite peaks completely

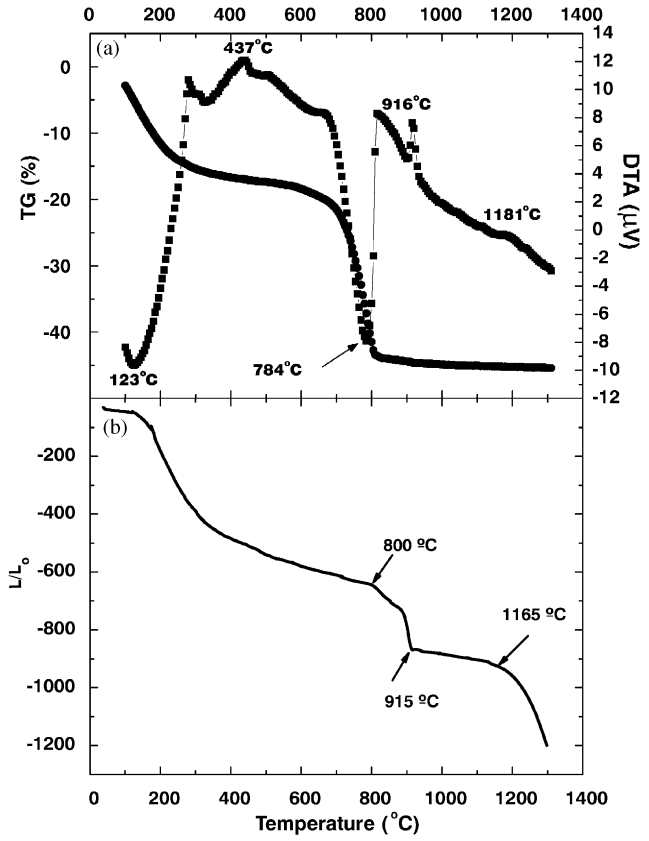

Fig. 2. Thermal records of a green compacted $CaCO_3$—amorphous $Al(OH)_3$ specimen when heated at a rate of 2°C/min. (a) Thermo-differential and thermogravimetric curves. (b) Constant heating rate dilatometry curve.

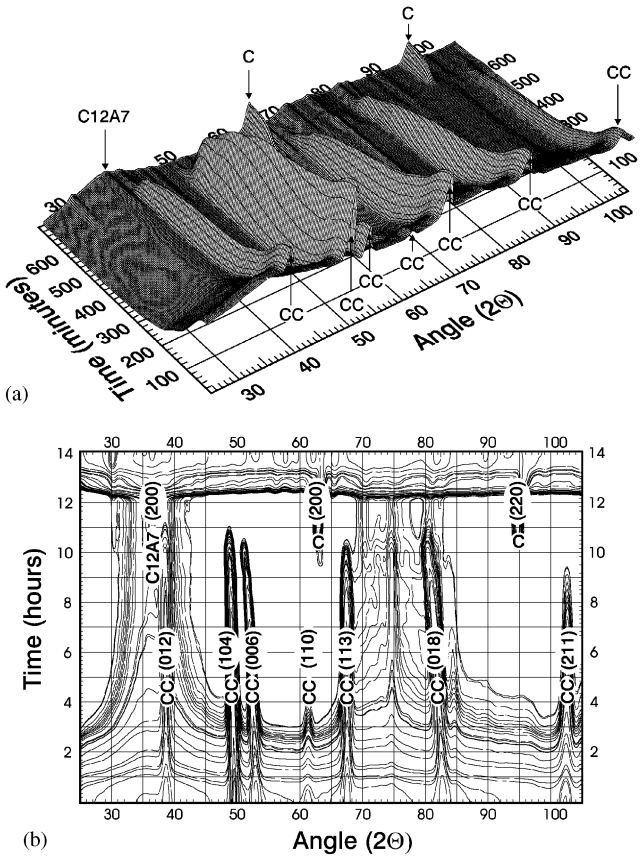

Fig. 3. The reaction sintering of a $CaCO_3$—amorphous $Al(OH)_3$. (a) Plot of neutron diffraction data collected during the heating cycle, represented as a sequence of patterns in a pseudo-three-dimensional fashion; in abscissae, diffraction angle (2Θ), in ordinate, time (minutes). (b) Contour map in two dimensions projected from the three dimensional surface. The diffraction peaks with their corresponding *hkl* indices are highlighted. The notation used correspond to the nomenclature used by cement chemists: CC stands for calcite, C12A7 for $Ca_{12}Al_{14}O_{33}$ and C for CaO.

disappeared by 800°C. The presence of a short-lived or intermediate phase such as CaO in the temperature range 750–900°C was observed too. The generation of $Ca_{12}Al_{14}O_{33}$ with an onset temperature ca. 900°C is also clear. The progressive peaks shift of $CaCO_3$ up to 660°C shows a thermal expansion anisotropy between *a* and *c* directions.

On the other hand, samples treated and quenched from temperatures ranging from 900°C to 1300°C (Table 2) were also studied by X-ray diffraction. See Fig. 4. In some of these specimens the transient phases $Ca_{12}Al_{14}O_{33}$ and $CaAl_2O_4$ were present. However phases such as $CaAl_4O_7$ and $CaAl_{12}O_{19}$ were not detected during the reaction process in any of the studied samples. The specimen treated at 1300°C did not show any trace of other crystal phases apart $Ca_3Al_2O_6$ itself.

3.4. Electron microscopy

The microstructure evolution with temperature was studied by scanning electron microscopy in samples treated at 1100°C and 1300°C during 1 min and subsequently quenched.

Samples heated at lower temperatures were not suitable to study them by this technique, as it will be explained with more detail during the discussion, because of the high reactivity of CaO.

Fig. 5 shows the fractured surfaces of specimens heated at 1100°C and 1300°C. It can be perceived a porous microstructure composed by

- Porous aggregates, $\simeq$2–5 μm in size, constituted by small crystallites ($\leqslant$500 nm) of CaO which did not react yet. These aggregates grew from the decomposition of $CaCO_3$ grains with an average size ranging from 8 to 15 μm.
- Areas with particles connected by necks, with a significant grain growth. In these areas $Ca_{12}Al_{14}O_{33}$ and $CaAl_2O_4$ spread in the interface between amorphous alumina and CaO.

Likewise, the sample treated at 1300°C, Figs. 5(c,d), shows significant sintering and considerable

Table 2
Phases identified by XRD analysis at different temperatures (°C)

Temperature	$CaCO_3$	$Al(OH)_3$	CaO	$Ca_{12}Al_{14}O_{33}$	$CaAl_2O_4$	$Ca_3Al_2O_6$
25	+ + +	+ + +	—	—	—	—
900	—	—	+ + +	+	—	—
1100	—	—	+ + +	+ +	+	—
1200	—	—	—	+	—	+ + +
1300	—	—	—	—	—	+ + +

The code used is Absent (−), little (+), fair (+ +) and abundant (+ + +).

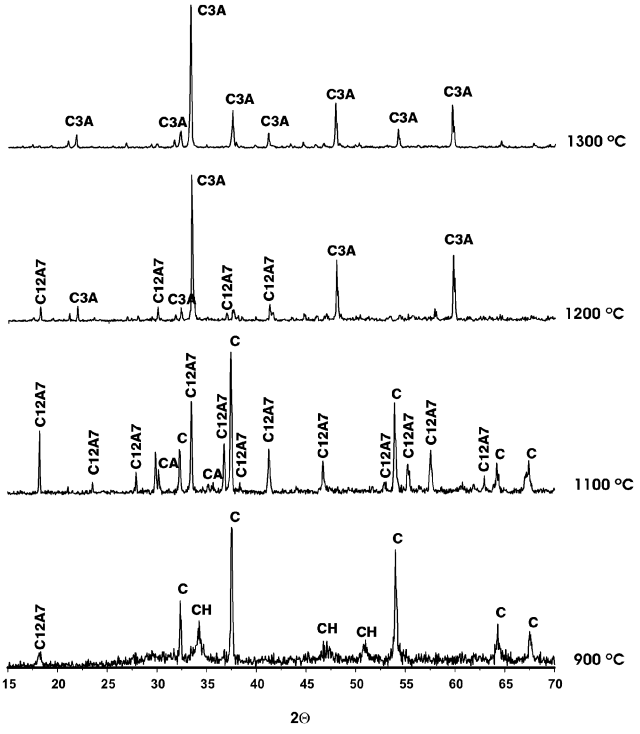

Fig. 4. X-ray diffraction patterns obtaining after quenching from the temperatures shown at the right side. Notation as in Fig. 3: C stands for CaO, CH for $Ca(OH)_2$, CA for $CaAl_2O_4$, C12A7 for $Ca_{12}Al_{14}O_{33}$ and C3A for $Ca_3Al_2O_6$.

increment in grain size, $\simeq 1$ μm. Again, particles seem to be connected by necks, but a distinctive morphology can be appreciated; pore channels seem to be formed by the coalescence of smaller ones. None of the specimens treated at 1300°C showed secondary phases.

4. Discussion

The synthesis was studied by neutron thermodiffractometry up to 1000°C only, for the reasons explained before. Basically, the most exciting events occur before that temperature, besides in this region exists CaO, whose avidity to capture water and/or CO_2 during an eventual quenching renders unfruitful any other exploration which is not *in situ*. Above that temperature it was judged that X-ray diffraction from quenched specimens would give enough information to follow the crystalline phases outcome.

On the other hand, the upper limit of temperature, 1300°C was established on the basis of the $CaO–Al_2O_3$ diagram which exhibits an eutectic at 1360 ± 5°C in the subsystem $Ca_3Al_2O_6/Ca_{12}Al_{14}O_{33}$. See Ref. [15,16]. This observation is compatible with the phase diagram. Special care must to be taken to avoid reaching the eutectic temperature since small deviations from the required stoichiometry can induce the development of undesired liquid phases in the vicinity of this invariant point. Also, in this particular case the presence of small sodium impurities (<0.2% by weight)—see Table 1—in the aluminum hydroxide could provoke a significant temperature decrease from the ideal one of 1360 ± 5°C.

The initial powder mixture was constituted by hard coarse $CaCO_3$ particles and "soft" amorphous aluminum hydroxide which were easily broken during the milling process (Fig. 1). The specific surface area of the calcite/amorphous aluminum hydroxide precursors increased around of 85% with milling. These increase in the specific surface area and decrease in the grain size facilitates the reaction process and minimize the possibility of forming chemical segregations as it was observed by other workers when studied the reaction sintering of samples with coarse grains of calcite. See Ref. [17].

The total loss of weight due to decomposition of reactants during the thermal treatment was calculated by the equation

$$\Delta W = \sum f_i \Delta W_i, \tag{2}$$

where f_i and ΔW_i are the weight fraction and weight loss, respectively, for every reactant. Using the data about the loss of weight of reactants, gathered in Table 1, it is possible to establish theoretical losses of 15.4% for the hydroxide and 28.8% for the carbonate. If we confront these values with the ones found from thermogravimetry, we can easily relate the first observed loss up to 300°C to the dehydration of aluminum hydroxide ($\approx 16\%$ vs. 15.4%) and the second between 700°C and 1200°C of $\approx 29\%$ to the calcite decomposi-

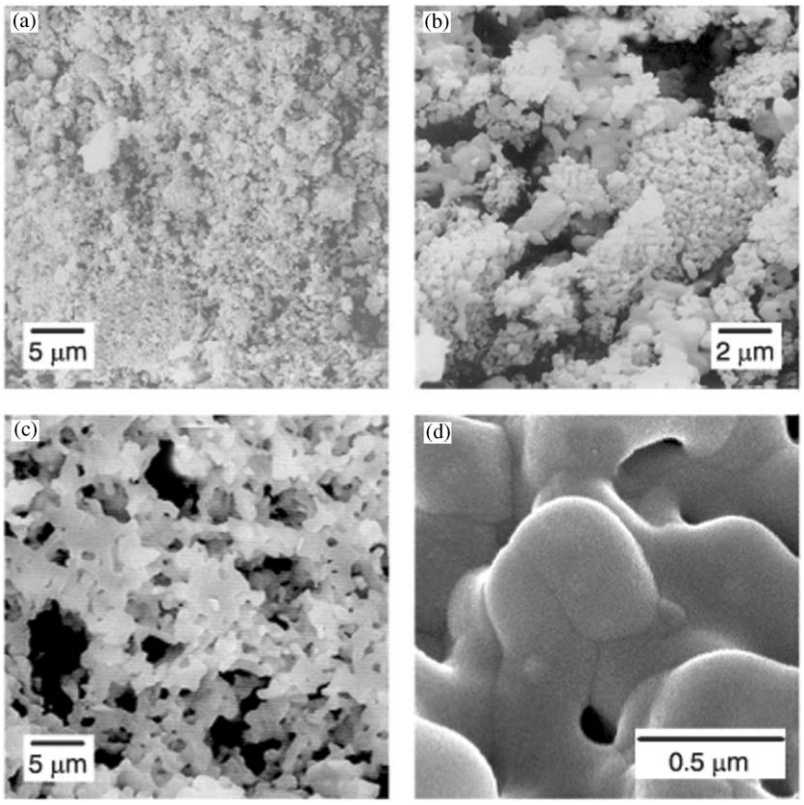

Fig. 5. Microstructural evolution of the specimen annealed at different temperatures as observed by back-scattered SEM on fractured surfaces. (a) and (b) are images of specimens annealed at 1100°C; (c) and (d) at 1300°C. In (b) an aggregate of CaO, at the right-hand side in the middle of the picture, can be seen. It was originated after thermal decomposition of bigger $CaCO_3$ grains. (c) and (d) exhibit a porous, fine-grained microstructure containing only $Ca_3Al_2O_6$ as determined by XRD. The progress of the reaction can be followed from the diffraction peaks. C stands for calcite, L for CaO and M for $Ca_{12}Al_{14}O_{33}$.

tion. Within the precision of the method, both values agree with the theoretical ones. If the global loss (encompassing the decomposition of both reactants) is considered, the slight discrepancy between the theoretical ($\approx 44.2\%$) and the observed ($\approx 45.4\%$) must be due to the volatilization of remaining isopropanol adsorbed to the surface of the powder. In fact, the wide exotherm with a maximum around 437°C is due, most likely, to the combustion of organic products.

These results seem to indicate that the reaction synthesis occurs faster and well before than the sintering process. They are in agreement with the works of Ali et al. [18] and Sing et al. [4]. According to them, the activation energy of sintering (698 kJ/mol) is much higher than the one of the synthesis from Al_2O_3–CaO mixtures (477 kJ/mol at 1200°C). Therefore it is clear that the reaction sintering proceeds in two well-differentiated steps: (a) reaction and (b) sintering of the products. Evidence arising from DTA-TG, dilatometry and XRD corroborates this two-stage trait. Furthermore, the neutron thermodiffractometry sequence of patterns allows to distinguishing clear-cut temperature regions, related to different phase transitions or reactions. These regions can be summarized as follows:

(1) The dehydration of amorphous aluminum hydroxide $Al(OH)_3$ is highlighted by the conspicuous decrease in the neutron diffraction patterns background due to the incoherent scattering of the hydrogen atoms present in amorphous $Al(OH)_3$, and by the thermal effects at 123°C in the TG and DTA curves (Fig. 2). This dehydration process

$$2Al(OH)_3 \rightarrow Al_2O_3(\kappa) + 3H_2O\uparrow \quad (3)$$

produces a cryptocrystalline (κ for short) phase, Al_2O_3, which neither XRD nor ND can detect. Only unreacted $CaCO_3$ is spotted by diffraction in this temperature region (Fig. 3).

(2) The decomposition of $CaCO_3$ to yield CaO plus CO_2 takes place between 700°C and 800°C, according to the equation,

$$CaCO_3 \rightarrow CaO + CO_2(g). \quad (4)$$

This is endothermic as DTA clearly reveals (Fig. 2). Also the parallel loss of weight in the TG plot and

Table 3
Thermodynamics calculations performed using the HSC thermochemical database, from 25°C to the temperature shown in the third column

Reaction	Eq. Ref. in text	Temperature (°C)	ΔG (kJ/mol)
$CaCO_3 \rightarrow CaO + CO_2(g)$	4	800	8
$Ca_{12}Al_{14}O_{33} + 9CaO \rightarrow 7Ca_3Al_2O_6$	9	1100	−28
$7CaAl_2O_4 + 5CaO \rightarrow Ca_{12}Al_{14}O_{33}$	8	1100	−30
$Al_2O_3 + CaO \rightarrow CaAl_2O_4$	7	1100	−41
$5Al_2O_3 + Ca_{12}Al_{14}O_{33} \rightarrow 12CaAl_2O_4$	6	1100	−174
$7Al_2O_3 + 12CaO \rightarrow Ca_{12}Al_{14}O_{33}$	5	900	−275

the collapse of neutron diffraction peaks confirm this (Fig. 3).

(3) The reaction between CaO and cryptocrystalline alumina starts at $\simeq$916°C. Unfortunately, cryptocrystalline alumina is undetected by diffraction probes, therefore evidence of its presence is circumstantial. It reacts with CaO through an expansive and exothermic reaction,

$$7Al_2O_3(\kappa) + 12CaO \rightarrow Ca_{12}Al_{14}O_{33} \quad (5)$$

forming a transient phase: $Ca_{12}Al_{14}O_{33}$ (see Figs. 2 and 3 and Table 3). The theoretical increment of volume due to mayenite formation is $\Delta V = 36.20\%$. The fast nucleation and growth of this solid transient phase, can be seen at the left-hand end of Fig. 3. The Gibbs free energy (ΔG) in the range 50–1300°C for the formation of phases involved in the reaction is shown in Fig. 6. Thermodynamic data indicate that reaction 4, has the lowest Gibbs free energy in the system CaO–Al_2O_3, and therefore is viable at lower temperatures than 916°C. However, as it is obvious the reaction does not happen until CaO is available once $CaCO_3$ decomposes.

(4) Formation of $CaAl_2O_4$ at 1100°C, as a transient phase produced by two reactions,

$$5Al_2O_3(\kappa) + Ca_{12}Al_{14}O_{33} \rightarrow 12CaAl_2O_4, \quad (6)$$

$$Al_2O_3(\kappa) + CaO \rightarrow CaAl_2O_4. \quad (7)$$

Thermodynamic calculations indicate that reaction 6 has the lowest Gibbs free energy hence it is the most favorable (Table 3).

(5) The formation of $Ca_3Al_2O_6$ takes place at about 1200°C. The following reactions are proposed to interpret the observation

$$7CaAl_2O_4 + 5CaO \rightarrow Ca_{12}Al_{14}O_{33}, \quad (8)$$

$$Ca_{12}Al_{14}O_{33} + 9CaO \rightarrow 7Ca_3Al_2O_6. \quad (9)$$

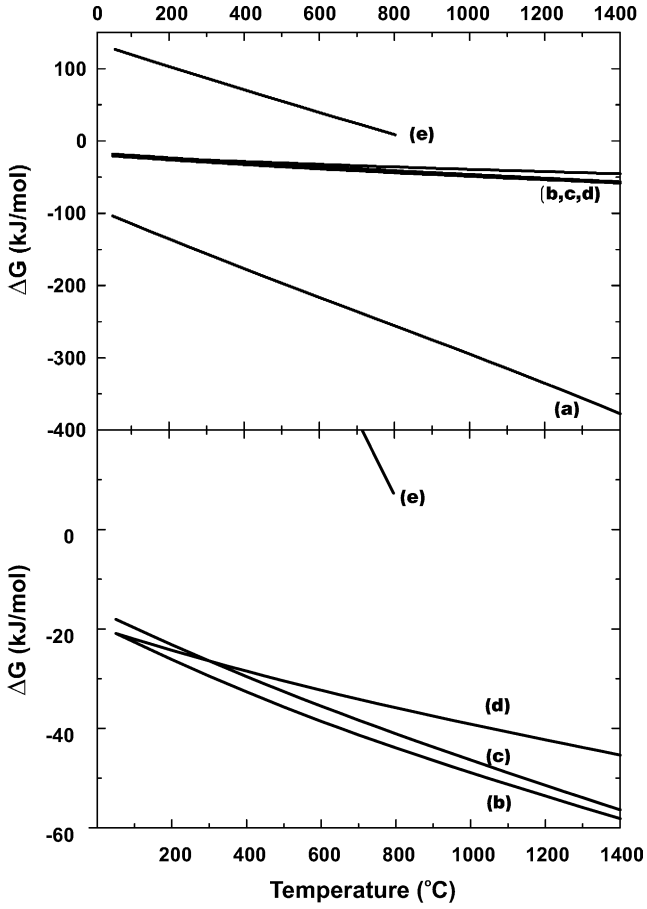

Fig. 6. Gibbs energy for the formation (from oxides) of phases involved in the reaction sintering process, plotted as a function of temperature. On top, the general trend for all, on the bottom, magnification to show with more detail their variations. (a) $Ca_{12}Al_{14}O_{33}$. (b) $CaAl_4O_7$ (c) $Ca_3Al_2O_6$. (d) $CaAl_2O_4$. (e) $CaCO_3$.

The present SEM studies do not support the hypothesis of liquid phase formation, see Figs. 5 and 6. On the other hand diffraction patterns show a flat background which corroborates the absence of vitreous phases. Therefore all evidence point at a solid-state mechanism for the reactions involved.

Thermodynamics calculations were used to validate the detailed model of the reaction sintering mechanism. Fig. 6 and Table 3 shows these free energy calculations for the reactions enumerated above. It can be appreciated that the theoretical predictions agree with the sequential appearance of phases. Namely, ΔG computations for the formation of $Ca_{12}Al_{14}O_{33}$, $CaAl_2O_4$ and $Ca_3Al_2O_6$ confirm the much lower ΔG value for $Ca_{12}Al_{14}O_{33}$ in the whole range of temperatures considered. Consequently, its appearance as the first phase during reaction is fully justified.

To summarize, the solid-state reactions between CaO and $Al_2O_3(\kappa)$ encompasses the nucleation of transient phases such as CaO, $Ca_{12}Al_{14}O_{33}$ and $CaAl_2O_4$ at

different points of the solid–solid interface. These nuclei grow in size and form a continuous reaction interface. Further reaction occurs by diffusion of reactants across the reaction interface which depends on the particle size, mixing ratio and reaction sintering temperature [19,20].

According to the present data and the works of Ali et al. [18] and Singh et al. [4], the reaction happens by diffusion of the ion with lower oxygen affinity, Ca^{2+}, into Al_2O_3 through a rigid oxygen lattice. Fig. 7 shows a scheme of the reaction mechanism. It may be explained in terms of the initial differences between the grain sizes of $CaCO_3$ and $Al(OH)_3$. At temperatures ca. 900°C, the larger $CaCO_3$ grains originate temporary porous CaO-segregations of 2–5 μm. See Figs. 5(a) and (b). The first formation of $Ca_{12}Al_{14}O_{33}$ occurs within the contacts between the small aggregates of CaO and amorphous alumina particles and may breed domains of $CaAl_2O_4$ and $Ca_{12}Al_{14}O_{33}$ of a few microns. At higher temperatures Ca^{2+} from the aggregates would diffuse through mayenite and $CaAl_2O_4$ layers to react and originate an homogeneous and porous single phase of $Ca_3Al_2O_6$ as a final product. The sintering process would take place at temperatures higher than 1200°C between grains of pure $Ca_3Al_2O_6$. Concerning the microstructure, the material sintered for 1 min at 1300°C exhibits a high porosity.

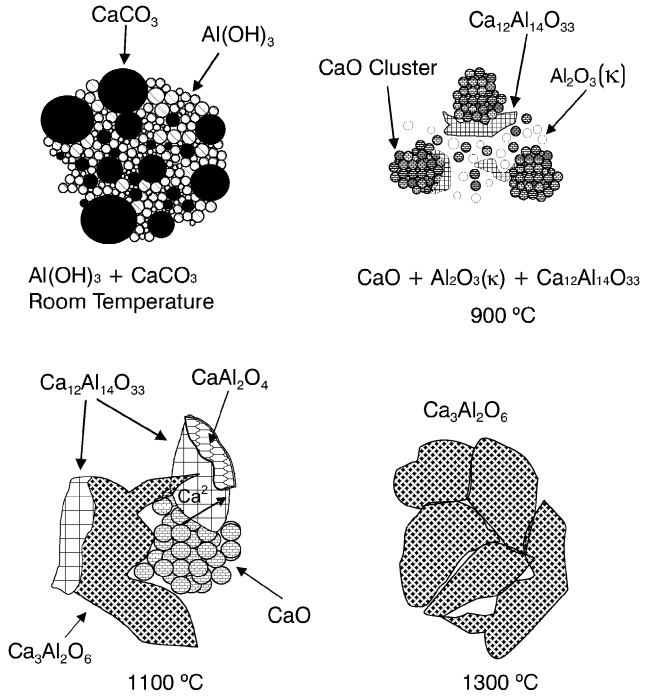

Fig. 7. Reaction mechanism sketch. At room temperature a uniform distribution of crystalline calcium carbonate and aluminum hydroxide is ready to react. After annealing at 900°C, $CaCO_3$ decomposes to yield CaO, in some cases as clusters (see Fig. 5(b)); also cryptocrystalline alumina and $Ca_{12}Al_{14}O_{33}$ are present. At 1100°C, Ca^{2+} diffuses towards alumina-rich phases to form $CaAl_2O_4$ (Eqs. (5) and (6) in main text) and $Ca_3Al_2O_6$. Finally at 1300°C the only phase present is $Ca_3Al_2O_6$.

The mechanism for the porosity development would be related to the release of H_2O and CO_2 during the dehydration of $Al(OH)_3$ and decomposition of $CaCO_3$. The evolved gases would yield an homogeneous open-pore structure with a narrow pore size distribution (Fig. 5(c)). Finally, it can be added that the experimental evidence indicated that the optimal temperature for reaction sintering of mechanochemically treated $CaCO_3$–$Al(OH)_3$ mixtures is around 1300°C, but to obtain a sintered compact, a dwell time at this temperature for at least 2 h is required.

5. Conclusions

Neutron thermodiffractometry with a 10°C resolution up to 950°C, combined to other techniques such as SEM, DTA-TG and XRD were used to determine the reaction mechanism during the high-temperature synthesis of $Ca_3Al_2O_6$ from mechanochemically treated $CaCO_3$ — amorphous $Al(OH)_3$ mixtures. The final step of the process takes place in two clear stages: reaction synthesis followed by sintering. The sequence of reactions observed during the heating ramp is in agreement with thermodynamic data. Transient crystal phases such as $Ca_{12}Al_{14}O_{33}$, CaO and $CaAl_2O_4$ are clearly spotted along the route to the final obtention of a porous, finely grained single phase of $Ca_3Al_2O_6$. This experiment has demonstrated the power of *in situ* neutron diffraction to reveal high-temperature reaction mechanisms and constitutes another contribution to the understanding of the ternary Ca–Al–O system from a dynamic or non-equilibrium perspective.

Acknowledgments

This research was partially supported by CICYT under the projects MAT-2000-0941 and CAM07N/0038-2001. We thank ILL for beamtime granted (experiment no. 5-25-83) and Dr. Javier Campo for his assistance in collecting ND data. One of the authors (JMRM) is indebted to the AECI for the fellowship awarded.

References

[1] P. Mondal, J.W. Jeffery, Acta Crystallogr. B 31 (1975) 689.
[2] A.C. Jupe, X. Turrillas, P. Barnes, S.L. Colston, C. Hall, D. Häusermann, M. Hanfland, Phys. Rev. B 53 (1996) R14697.
[3] J. Williamson, E.P. Glasser, J. Appl. Chem. 12 (1962) 535.
[4] V.K. Singh, M.M. Ali, U.K. Mandal, J. Am. Ceram. Soc. 73 (1990) 872.
[5] B.M. Mohamed, J.H. Sharp, Thermochim. Acta 388 (2002) 105.

[6] A.M. Ginstling, B.I. Brounshtein, Zh. Prikl. Khim 23 (1950) 1327 [Cfr. in: C.H. Bamford, C.F.H. Tipper (Eds.), Reactions in the Solid State, Vol. 22, Elsevier, Amsterdam, 1980, pp. 301].
[7] J. Temuujin, K.J.D. MacKenzie, T. Jadambaa, B. Namjildorj, B. Olziiburen, M.E. Smithe, P. Angererf, J. Mater. Chem. 10 (2000) 1019.
[8] J. Temuujin, K.J.D. Mackenzie, J. Eur. Ceram. Soc. 18 (1998) 831.
[9] M. Senna, Solid State Ionics 63–65 (1993) 3.
[10] Outokumpu Research Oy, Pori, Finland Outokumpu HSC Chemistry for Windows Version 1.10., 1993.
[11] A.H. de Aza, M.A. Rodríguez, S. De Aza, P. Pena, P. Convert, T. Hansen, X. Turrillas, J. Am. Ceram. Soc. 85 (2002) 881.
[12] OriginLab Corporation, Northampton, Ma, 01060, USA, Program Origin Version 5.0, 1999, www.OriginLab.com
[13] Research Systems Inc. (Kodak Company), Sterling, Va, 20164, USA, Program NOeSYS, Version 1.2, 1998, www.rsinc.com
[14] Research Systems Inc. (Kodak Company), Sterling, Va, 20164, USA, Program IDL Version 5.2, 1998, www.rsinc.com
[15] R.W. Nurse, J.H. Welch, A.J. Majundar, Trans. Br. Ceram. Soc. 64 (1965) 409.
[16] B. Halstedt, J. Am. Ceram. Soc. 73 (1990) 15.
[17] V.K. Singh, U.K. Mandal, Trans. J. Br. Ceram. Soc. 81 (1982) 112.
[18] M.M. Ali, S.K. Agarwal, S.K. Handoo, Cem. Concr. Res. 27 (1997) 979.
[19] J.L. Rodríguez, S. De Aza, P. Pena, Br. Ceram. Trans. 100 (2001) 181.
[20] J.L. Rodríguez, P. Pena, Bol. Soc. Esp. Cerám. Vidrio 40 (2001) 463.